Piezoelectric polyacrylonitrile nanofiber film based dual-function self-powered flexible sensor

Gengrui Zhao[†‡], Xiaodi Zhang[†‡], Xin Cui[¶], Shu Wang[†‡], Zhirong Liu[†‡], Lin Deng[†‡], Anhui Qi[†], Xiran Qiao[†], Lijie Li[§], Caofeng Pan[†‡¶], Yan Zhang[⊥†¶], Linlin Li[†‡¶*]*

[†] Beijing Institute of Nanoenergy and Nanosystems, Chinese Academy of Sciences, Beijing 100083, P. R. China

[‡] School of Nanoscience and Technology, University of Chinese Academy of Sciences, Beijing 100049, P. R. China

[¶] Center on Nanoenergy Research, School of Physical Science and Technology, Guangxi University, Nanning 530004, P. R. China

[§] Multidisciplinary Nanotechnology Center, College of Engineering, Swansea University, Bay Campus, Swansea SA1 8EN, United Kingdom

[⊥] School of Physics, University of Electronic Science and Technology of China, Chengdu 610054, P. R. China

KEYWORDS: self-powered, electrospinning, triboelectric nanogenerator, piezoelectric effect, flexible sensor

ABSTRACT: To meet the growing demands in flexible and wearable electronics, various sensors have been designed for detecting and monitoring the physical quantity changes.

However, most of these sensors can only detect one certain kind of physical quantity based on a single mechanism. In this paper, we have fabricated a multifunctional sensor made from carbonized electrospun polyacrylonitrile/barium titanate (PAN-C/BTO) nanofiber film. It can detect two physical quantities (pressure and curvature), independently and simultaneously, by integrating piezoresistive, piezoelectric and triboelectric effect. For flex sensing with the impedance change of PAN-C/BTO nanofiber films during bending, it had a sensitivity of 1.12 deg^{-1} from 58.9° to 120.2 ° and a working range of 28°~150°. For self-powered force sensing, it had a gauge factor of 1.44 $V \cdot N^{-1}$ within the range of 0.15~25 N. The sensor had a long stability over 60,000 cycles at both sensing modes. The inclusion of barium titanate nanoparticles (BTO NPs) into the nanofiber film had an over 2.4 times enchantment of sensitivity for the pressure sensing due to the synergy of piezoelectric and triboelectric effect. Based on the multifunction and modularity, a series of potential applications of the sensor were demonstrated, including sensing human's swallowing, walking gaits, finger flexure and finger-tapping sensitively. The self-powered flexible dual-mode sensor has great application potential in human-computer interactive and smart wearable sensing system.

1. INTRODUCTION

In recent years, flexible and wearable electronics have attracted great interests with their miniaturization, portability and potential applications in human-machine interface (HMI) and internet of things (IoT). Especially, several branches of flexible electronics, such as E-skin,[1-2] wearable sensors,[3-4] and wearable energy harvesting/storage device,[5-7] have obtained considerable development. As basic devices, flexible sensors play an important role in detecting substance in environment and the changes of physical quantities, and extending sensory scope of human. Diverse flexible sensors have been proposed to detect heat,[8] force,[9] strain,[10] and chemicals,[11] *etc*. The human physical indicators detected by flexible sensors include heart/pulse beating,[12] eyes blinking,[13] and limbs bending,[10] *etc*. A certain sensor often

detects one certain physical change and collects the signals to further help people control the physical change in turn, and thus achieves the interaction between human and machines.

Many kinds of flexible force sensors derived from different materials, such as metal nanowires,[14-15] carbon nanotubes- or graphene-based materials,[4, 16] and porous foam conducting materials[17] have been proposed. The working mechanisms of the flexible force sensors are mainly based on resistive,[15, 18] piezoelectric,[19-20] and capacitive effect.[4, 14] More recently, self-powered flexible and wearable sensors based on triboelectric nanogenerator (TENG) have become a research hotpot with the advantages of self-power, broad materials selection, various structure designs, high sensitivity and diverse applications.[21-23] However, these sensors can often work on the basis of a single mechanism with limited detection parameter and detection sensitivity. For example, traditional piezoresistive or piezoelectric sensor can only detect strain or pressure. In order to meet the requirements for different applications, the development of multipurpose sensors with the ability to sensitively detect multiple parameters is urgently desired. A few researches are only been reported very recently. For instance, Wang's group have built a self-powered pressure sensing system integrating the resistive sensor and TENG sensor.[24] Wang *et al.* proposed a dual-mode tactile sensor working in piezoresistive sensory mode and self-powered TENG sensory mode.[17] Lee's group developed a dual-mode amenity force/humidity sensor based on the water-air TENG by characterizing two independent charge transfers.[25]

In this study, we have fabricated a multifunctional flexible sensor that can detect pressure and curvature independently and simultaneously by the integration of piezoelectric, triboelectric, and piezoresistive effect together. Fabricated by a convenient electrospinning, carbonization and encapsulation process, the carbonized PAN/$BaTiO_3$ nanofiber (PAN-C/BTO) based sensor can detect curvature based on resistive mode, and pressure based on the single electrode TENG mechanism independently. With BTO NPs integrated into the carbonized PAN

nanofibers, the output voltage and current of the flexible PAN-C/BTO based sensor was greatly enhanced when working as a force sensor at a single electrode TENG mode. As the first flexible dual-function sensor innovatively integrating the curvature measurement with pressure force sensing, the PAN-C/BTO nanofiber based sensor was applied for human gesture capture, physical detection, and motion sensing. It has potential applications in intelligent sensing system and HMI technology.

2. EXPERIMENTAL SECTION

2.1. Preparation of the PAN/BTO Nanofiber Films. 0.4 g polyacrylonitrile (PAN) (Mw=15,000, Macklin) and 0.1 g $BaTiO_3$ nanoparticles (BTO NPs, Sigma-Aldrich) were added into 3.6 g N,N-Dimethyl Formamide (DMF, 99.8 %, AcroSeal). The mixture was ultrasonic for 2 h after 1 h magnetic stirring, and then poured into a 10 mL syringe for electrospinning. The lab-build electrospinning setup has a plate collector that was 15 cm away from the 25 G needle. A 15 kV high voltage was applied between the syringe needle and the collector. The electrospinning process was carried out at 25 ^{o}C, 30% RH humidity, and 1 mL/h injection rate. The as-spun PAN/BTO nanofiber films were dry for 4 h at 60 ^{o}C to volatilize the residual solvent. For PAN nanofiber films, the electrospinning was performed without the addition of BTO NPs.

2.2. Fabrication of the Flexible Dual-function Sensor. The PAN/BTO nanofiber films were heated in a tube furnace from room temperature (RT) to 240 ^{o}C with a heating rate of 5 ^{o}C min^{-1}, and stabilized at 240 ^{o}C for 4 h in the ambient air. Then, the furnace was perfused with protective gas of argon and the temperature was increased to 700 ^{o}C with a rate of 2 ^{o}C min^{-1} and kept for 1 h to carbonize the nanofiber films. During the course of temperature cooling to room temperature, the argon atmosphere was maintained. The carbonized PAN-C/BTO nanofiber films were cut into rectangular strips (1.5 cm ×1.5 cm) and connected to copper leads at two counter ends with silver paste. It was put on a polydimethylsiloxane (PDMS, fabricated

with a 10:1 mixture of base and curing agent, Dow Corning Sylgard 184) thin film (2 cm×2 cm in size; 1 mm thick), and then liquid PDMS was smoothly covered onto the surface to encapsulate the device. Finally, the samples were cured at 80 ºC for 3 h. The final sensors had a size of 2 cm×2 cm and thickness of ~2 mm.

2.3. Characterizations and Performances. The morphology and structure of the nanofiber films were characterized by a field emission scanning electron microscope (FE-SEM, Hitachi, SU-8020) and a high resolution transmission electron microscope (HRTEM, Tecnai G2). X-ray diffraction (XRD) patterns were carried out by a PANalytical X'pert^3 Powder diffractometer using a CuKα source with a step size of 0.013° and recorded over an angular range from 10° to 80°. Raman spectra were performed on a Raman spectroscope (HORIBA HR800) with a laser excitation wavelength of 532 nm. The bending deformation of the sensor was performed with a linear motor (Linmot), and the electrical signals of the strain were recorded at the same time by a Keithley 2400 digital meter at a constant voltage of 5 V. The pressure force applied on the sensor was monitored by a commercial sensor (501F01, YMC Pizeotronics INC) mounted on the motion part of the linear motor, while the triboelectric output of the self-powered sensor was recorded by a Keithley 6514 electrometer.

3. RESULTS AND DISCUSSION

Electrospinning is a facile and convenient technique to produce nanofibers, especially for polymer materials. Importantly, inorganic nanoparticles with special physicochemical properties could be incorporated to form composite nanofibers by choosing a suitable solvent to solve the polymer molecules and disperse the inorganic nanoparticles concurrently. **Figure 1**a shows the fabrication process of the dual-function PAN-C/BTO based sensors. The PAN/BTO nanofibers were electrospun from PAN solution mixed with BTO nanoparticles, and then carbonized under Ar atmosphere to endow it with good conductivity. The sensors were

obtained by PDMS encapsulation of the PAN-C/BTO nanofiber film connected with copper wires at two terminals. Herein, randomly aligned nanofibers were fabricated using a flat plate collector, ensuring the generation of many mesoscopic joints with enhanced mechanical robustness. It was not as vulnerable as the oriented one that tended to be tore apart along the alignment direction.[26] From the scanning electron microscopy (SEM) image, the as-spun PAN/BTO nanofiber films had a randomly oriented structure with nanofiber diameter of ~400 nm (Figure S1 in Supporting Information). Although protrusions could be observed, the as-spun nanofibers had a smooth surface, straight shape and had no conglutination between each other. After 700 ^{o}C treatment in the argon protection environment, the PAN nanofibers were carbonized (PAN-C/BTO). The whole nanofiber films turned into black from as-spun white, and the overall dimension was reduced (Figure S2 in Supporting Information). The carbonated PAN-C/BTO nanofiber had a rough surface and many protrusions on the fiber surface. Especially, nanofibers were joined together at the criss-cross and overlaps, becoming curlier like twisted roots (Figure 1b). The diameter of the nanofiber became uneven after carbonization. The overall mean diameter was ~160 nm, much less than that before carbonization. The protrusions were caused by the heterogeneous distribution of BTO NPs during the formation of nanofibers (Figure 1b inset). Furthermore, a single PAN-C/BTO nanofiber was observed by transmission electron microscope (TEM) to discern the precise nanostructure (Figure 1c and inset). BTO NPs had a lattice fringe d_{110}= 2.8Å, consistent with the crystal structure of original tetragonal BTO NPs (Figure S3 in Supporting Information). They were aggregated to form a protrusion on the surface of the amorphous nanofiber.[27] Actually, the aggregation of BTO NPs was conducive to enhance the piezoelectric output power generation, because the protrusions had a larger volume to effectively harvest external applied mechanical stress and increase the total dipole moment.[28] Energy Dispersive X-Ray Spectroscopy reveals that BTO NPs (element of Ba and Ti) were embedded in the carbonized nanofiber (Figure 1d-i). It was worth noting

that O existed not only in BTO NPs, but also in the carbonized nanofiber, which was caused by the oxidation of carbon fiber in the air at 240 °C.

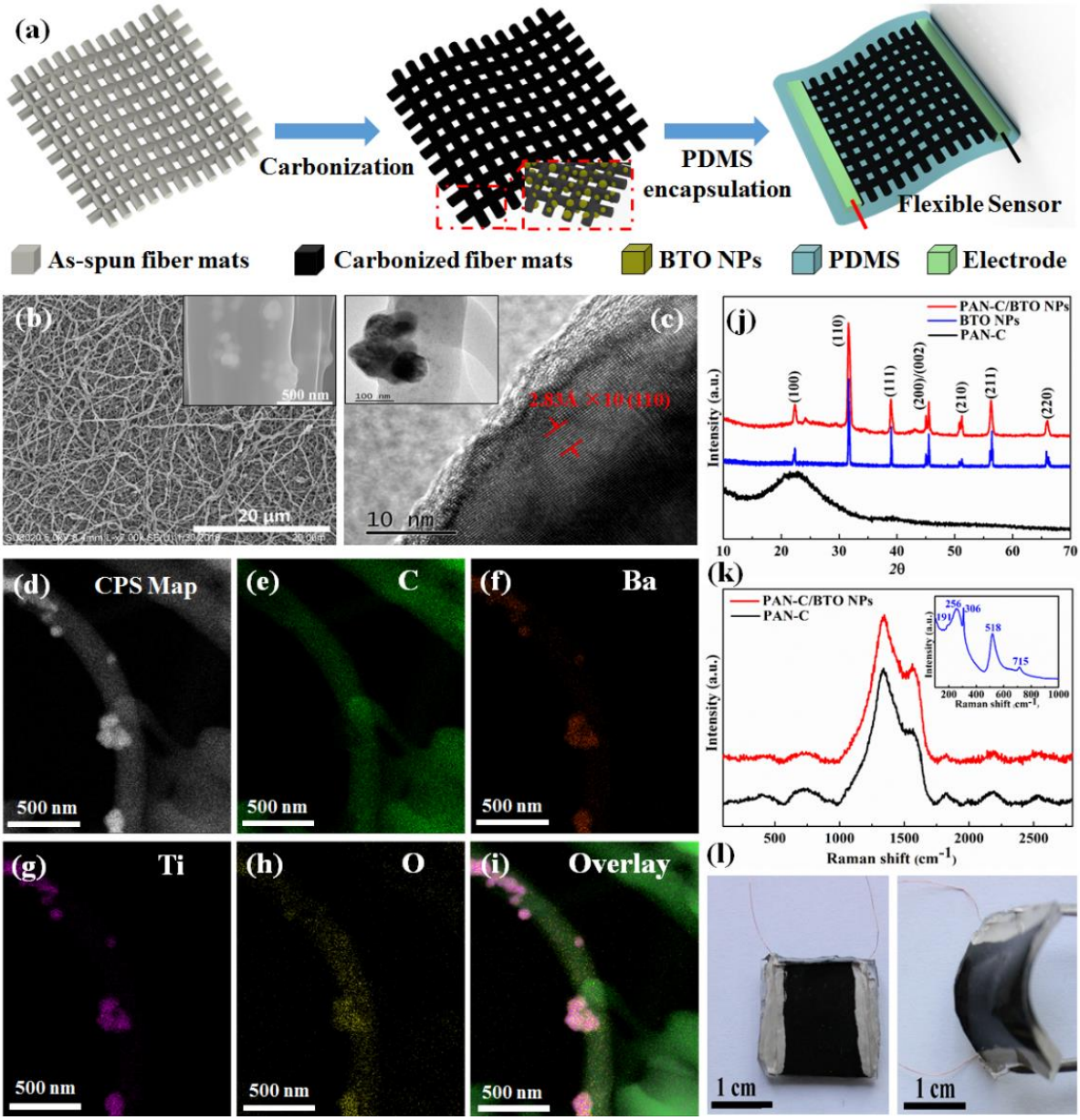

Figure 1. Flexible multifunctional PAN-C/BTO sensor. a) Illustration showing the fabrication process of the PAN-C/BTO based sensor. b) SEM image of carbonized PAN/ BTO nanofibers. c) TEM image of carbonized PAN/BTO nanofibers. d-i) EDX images of a single carbonized PAN-C/ BTO nanofiber. j) XRD curves of PAN-C, PAN-C/BTO nanofiber films and BTO NPs. k) Raman spectra of PAN-C and PAN-C/BTO nanofiber films, the inset shows the BTO nanoparticles. l) Photograph of a flexible dual-function PAN-C/ BTO based sensor.

X-ray diffraction (XRD) spectrum also proved that the PAN-C nanofiber had an amorphous structure with carbon peak centered at 23° (Figure 1j). PAN-C/BTO nanofibers had characteristic peaks corresponding to the (100), (110), (111), (200), (210), (211), and (220) planes of crystalline BTO, identical to free BTO NPs.[29-32] It is noteworthy that the peak splitting at 45° for (200) and (002) planes indicated that the BTO NPs had a tetragonal phase with piezoelectric effect (Figure 1j).[33-34] PAN-C nanofibers (carbonized PAN nanofibers without BTO NPs) and PAN-C/BTO nanofibers showed similar Raman spectrum patterns with peaks at 1360 cm^{-1} (defects or heteroatom doping (D-band)), and 1580 cm^{-1} (crystalline sp2 carbon (G-band)) (Figure 1K). [35] The D-band peak was higher than the G-band peak, indicating that the nanofiber films had a defective or heteroatom doped graphene structure. The I_d/I_g value of the PAN-C/BTO nanofibers was about 1.9. For PAN-based carbonized nanofibers, the conductivity was reported to increase with the pyrolysis temperature, and also increased considerably with the pyrolysis time at lower pyrolysis temperature.[36-37] No peaks corresponding to tetragonal BTO (Figure 1k inset) was observed for PAN-C/BTO nanofibers, which may be attributed to the low percentage of BTO NPs. If we analysis the Raman spectrum of BTO nanoparticles solely, the characteristic peaks of tetragonal phase could be observed in the range of 100~1000 cm^{-1} (Figure 2f inset). The peaks at 191 cm^{-1} [A_1(TO), E(LO)], 256 cm^{-1} [A_1(TO)], 306 cm^{-1}[B_1, E(TO+LO)], 518 cm^{-1} [E, A_1(TO)], and 715 cm^{-1} [A_1,E(LO)] were all subjective to the tetragonal phase of BTO NPs. [27-28]

The two terminals of the carbonized nanofiber films were connected with copper wires by silver paste, respectively, and encapsulated by polydimethylsiloxane (PDMS) (Figure 1l). PDMS is a kind of low-cost, simple to use, chemically inert polymer. In view of the flexibility and biocompatibility of cured PDMS, it has been extensively applied in wearable electronic devices.[22, 38-39] The final device had a size of 2×2 cm, thickness of 2 mm with good flexibility (Figure 1l). Because of the PDMS encapsulation, the PAN-C/BTO based sensor was water-

proof. After been immersed in water for 10 min, the output signal of the dried sensor was not affected (Figure S4 in Supporting Information).

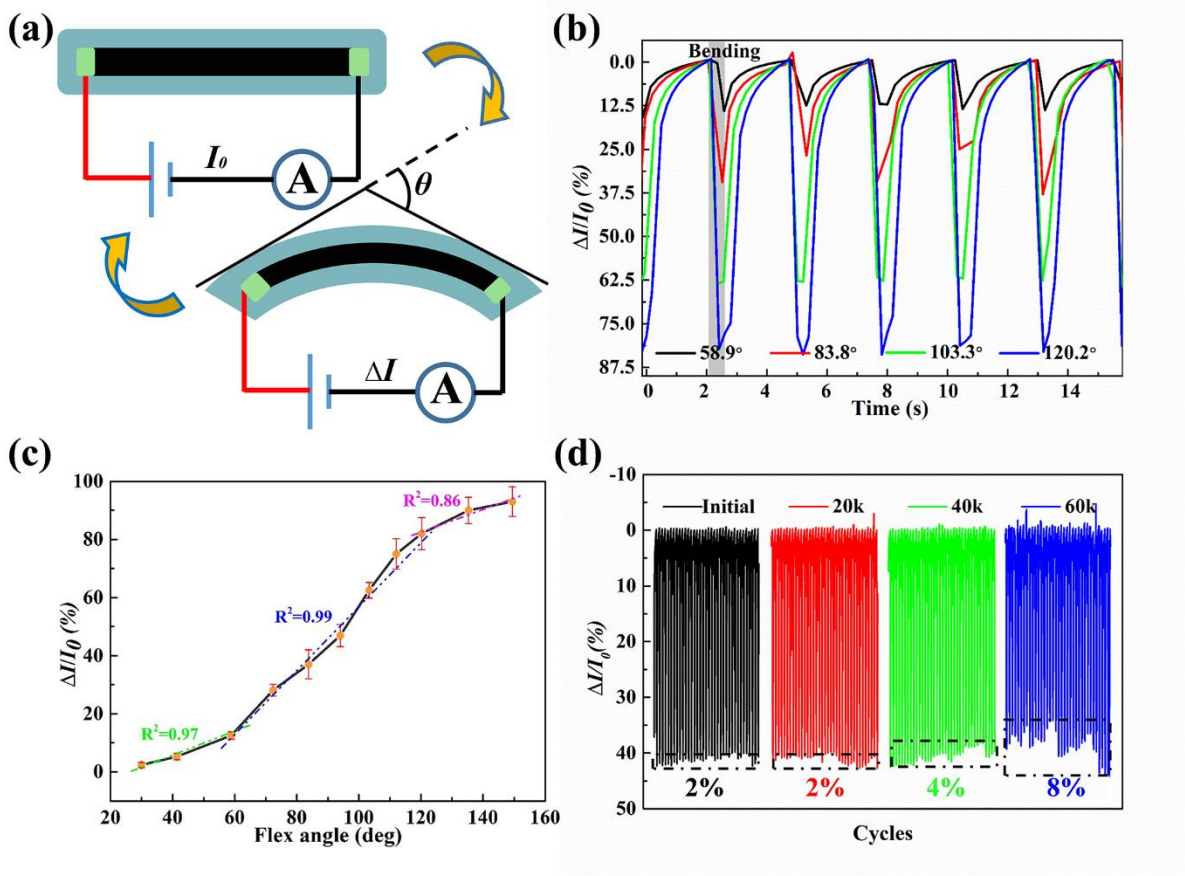

Figure 2. The electromechanical properties of the PAN-C/BTO based sensor working as a flex sensor at resistance mode. a) The working schematic diagram of the PAN-C/BTO based sensor working as a flex sensor. b) Curves of relative change in current when the flex sensor working at 58.9°, 83.8°, 103.3° and 120.2° of flex angle. c) Relative change in current of the flex sensor versus the flex angle. d) Relative change in current under repeated bending and releasing of 90° for 60,000 cycles, showing the durability of the sensor. The changes of $\Delta I/I_0$ was within 2% after 20,000 bending-releasing cycles, 4% after 40,000 cycles, and 8% after 60,000 cycles, respectively.

The flexible sensor based on PDMS encapsulated PAN-C/BTO could work for the detection of motions including bending and pressing. The schematic of testing setup is shown in Figure

S5 in Supporting Information. The flex sensor was bended when force was applied on its both ends, and the bending degree could be defined by flex angle (**Figure 2**a). In our experiment, the bending of the flex sensor was performed by pushing inward the two free ends of the sensor (Figure S5). The sensing principle was based on the impedance change of the conducting nanofiber film. The bending deformation of the sensor led to the bend and stretch of the conducting nanofiber film, thus increasing the resistance. When the deformation was recovered, the conducting fiber layer returned to their initial state and the resistance came back to the unbending state. It was noteworthy that the conductivity of PAN-C/BTO nanofiber film was comparable (~10.25 kΩ sq^{-1}) to the PAN-C nanofiber film (~6.54 kΩ sq^{-1}). Because of the flexible encapsulating material, conducting nanofiber layer was supported and restricted during bending deformation so that it would not be broken. Similar to the resistive strain gauges, here we defined the gauge factor (GF) as the relative change in current divided by the flex angle：

$$GF=\frac{\Delta I}{I_0\theta} \quad (1)$$

$$\Delta I=|I-I_0| \quad (2)$$

Where I is the real-time current when the sensor bending, and I_0 is the current of sensor without bending, and θ is the flex angle. ΔI is the absolute value of the difference between current at bending and releasing. Figure 2b is a real-time measurement of the relative change of current ($\Delta I/I_0$) under a series of flex angles at 58.9°, 83.8°, 103.3° and 120.2° for the PAN-C/BTO based flex sensor. In comparison, the real-time $\Delta I/I_0$ curves of the PAN-C based flex sensor at the same bending angles are shown in Figure S6. The PAN-C based flex sensor had a similar signal strength with that of the PAN-C/BTO based one, indicating the doping of BTO NPs didn't affect the sensitivity of the flex sensor. The relationship between $\Delta I/I_0$ and angle magnitude is plotted in Figure 4c. When the flex angel of the sensor increased from 28° to 150°, the $\Delta I/I_0$ significantly increased from 2% to 92%, along with the resistance increase of the conducting nanofiber layer. The gauge factors of the flex sensor were calculated by separating

the flex angle into 3 angle ranges and fitting the curve, to be 0.36 deg^{-1} from 30° to 58.9 °, 1.12 deg^{-1} from 58.9° to 120.2 °, 0.37 deg^{-1} from 120.2° to 149.4°, respectively. To further demonstrate the stability of the flex sensor, a continuous bending cycle of 90° was applied to the sensor. The sensor maintained a high signal-to-noise ratio, and the changes of $\Delta I/I_0$ was within 2% after 20,000 bending-releasing cycles, 4% after 40,000 cycles, and 8% after 60,000 cycles, respectively (Figure 2d). The fluctuation could be attributed to the slight fatigue wear. Furthermore, as a flex sensor, it also could detect applied force during bending. In the bending-releasing process, a horizontal impulse force was applied onto the sensor at bending and releasing status, respectively. Because the horizontal impulse force affected the curvature of the sensor, new peaks could be distinguished in both bending and releasing signal curves (Figure S7 in Supporting Information). At the extreme position of bending, a small reverse peak appeared at the original signal peak maximum. It was because the horizon force impeded bending, inducing a ~5% $\Delta I/I_0$ signal degradation. At the releasing status, the horizon force caused the slight bending, so a small peak appeared, which represented a 8% $\Delta I/I_0$ signal generation. It suggested that the flexible sensor could achieve a sensitive tactile detection during curvature sensing.

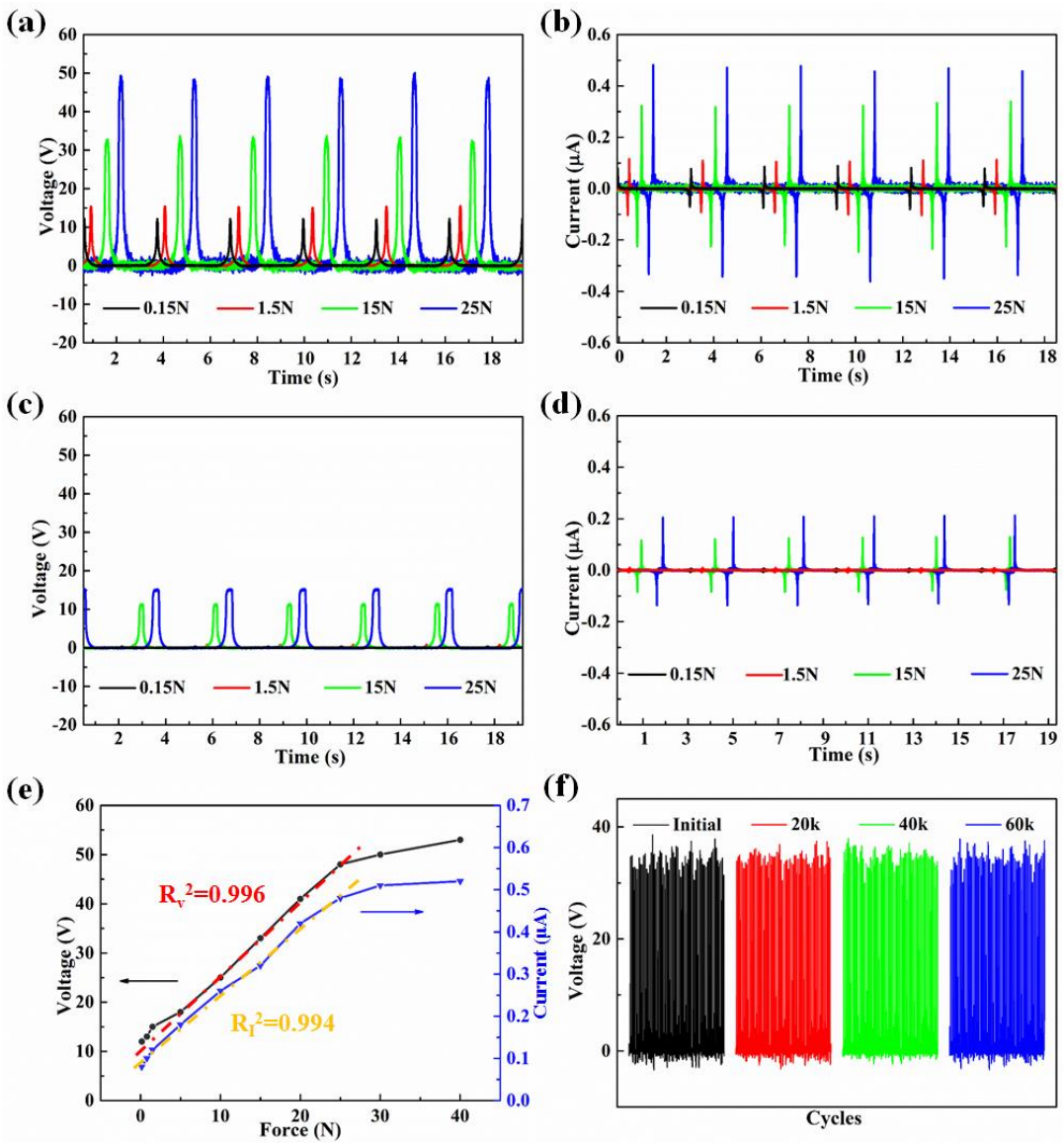

Figure 3. The PAN-C/BTO based sensor and PAN-C based sensor working as a self-powered pressure sensor at the triboelectric mode. The open-circuit voltage (a) and short-circuit current (b) of the PAN-C/BTO based pressure sensor. The open-circuit voltage (c) and short-circuit current (d) of the PAN-C based pressure sensor. They shows that the PAN-C/BTO based pressure sensor has a higher V_{oc} and I_{sc} signal than that of the PAN-C based pressure sensor. e) The open-circuit voltage and short-circuit current of the PAN-C/BTO self-powered pressure sensor under different pressure force. f) The voltage signal under repeated loading and unloading of a 15 N impulse force for 60,000 cycles, showing the durability of the self-powered pressure sensor.

As a dual-function flexible sensor, it can not only detect bending angle in a large range, but also work for self-powered pressure sensing. When the sensor worked for pressure sensing, it was in essence as a single-electrode triboelectric nanogenerator (SE-TENG). The flexible encapsulating material of PDMS worked as a dielectric layer to produce an electrical charge by the contact electrification, and the carbonized nanofiber layer acted as an electrode to collect those charge and conducting current. In the measurement process, a piece of clean and smooth Kapton film (Φ11.5 mm) was stuck on a commercial force sensor as the active part to contact with the PAN-C/BTO sensor. The commercial force sensor had an 11.5 mm diameter with the end face as the stress surface, so the contact area of the forcing punch was a Φ11.5 mm circular area. As previously mentioned, the flexible sensor had a 2×2 cm rectangular PDMS surface. The self-leveling PDMS had a smooth and clean surface after curing. The schematic of measurement setup for the self-powered force sensor is shown in Figure S5. An impulse force was applied onto the sensor surface to measure the actual force by a linear motor. Two independent sensors were measured, one with PAN-C/BTO NPs nanofiber and the second of PAN-C nanofiber without BTO NPs. The real-time measurement result of open-circuit voltage (V_{oc}) and short-circuit current (I_{sc}) of the PAN-C/BTO based sensor, under various pressures is shown in **Figure 3a-b**. The PAN-C/BTO based sensor had a V_{oc}/I_{sc} electric output of 12 V /0.08 μA, 15 V /0.11 μA, 32 V /0.32 μA, and 49 V/0.48 μA under 0.15 N, 1.5 N, 15 N, and 25 N impulse force, respectively. Compared to the PAN-C/BTO based sensor, the PAN-C based sensor had a lower electric output under the same pressure (2.7~12 times lower in V_{oc}, and 2.3~13 times lower in I_{sc} under different pressures). Its V_{oc} were 1V, 2V, 12V and 15V, while the I_{sc} were 6 nA, 13 nA, 120 nA and 205 nA under 0.15 N, 1.5 N, 15 N, and 25 N impulse force, respectively (Figure 3c-d). It was speculated that remarkable signal enhancement of the PAN-C/BTO based sensor was owing to the piezoelectric effect of BTO NPs embedded in the carbonized nanofiber. The relationship between V_{oc}, I_{sc} and magnitude of angle is plotted in

Figure 3e. There was a favorable linear relationship between electric output (R_V^2=0.996 for V_{oc} or R_I^2=0.994 for I_{sc}) and force from 0.15 N to 25 N, indicating the PAN-C/BTO based sensor was reliable for force detecting. The triboelectric outputs increased with the increasing of pressure, which may be attributed to the largened contact area. When a rigid counterpart material was pressed on the soft PDMS with increased pressure, the contact area would also increase due to the microcosmic deformation of PDMS. When the pressure increased to a certain extent, the PDMS was compressed to a threshold and the contact area would not increase anymore. So the triboelectric outputs had no significant increase when the pressure was higher than 25 N. Similarly, the sensitivity of the force sensor is defined by the equation of

$$GF=\frac{V_{oc}}{F} \quad (3)$$

Where V_{oc} is the open-circuit voltage when pressure is applied on the sensor, and F is the applied pressure. The calculated gauge factor of the force sensor was 1.44 $V \cdot N^{-1}$ within the range of 0.15~25 N. As a single-electrode triboelectric nanogenerator, its triboelectric output is largely dependent on the opposite material. In different usage environments, the triboelectric output would be affected by temperature, humidity and surface properties of opposite material. Therefore, before using the PAN-C/BTO based sensor to accurately measure force, calibration should be performed in advance.

As a pressure sensor, the PAN-C/BTO sensor is commonly put on a flat surface, which would not bend under pressure. In some circumstances, the sensor may bend while applying force. To simulate, the two terminal ends of the sensor was supported by two stands, allowing the sensor to bend under pressure (Figure S8). From the real-time V_{oc} curves of the sensor under pressure with bending and without bending, the V_{oc} of the bent sensor under pressure was slightly lower than that without bending, because the sensor could not sufficiently contact with counterpart. Furthermore, the peak of the bent sensor oscillated at the high voltage value for longer time,

because of the longer contact time during the bending deformation of the sensor. The PAN-C/BTO based sensor also had an extraordinary stability when it working at the TENG mode. The triboelectric output had no obvious change after 60,000 pressure loading-unloading cycles (Figure 3f).

Tetragonal barium titanium nanocrystal has a crystal structure with one body-centered Ti atom, six face centered O atoms and eight Ba atoms at each corner (**Figure 4**a). When the BTO is subjected to a mechanical stress, it is poled by structural deformation to generate a local piezoelectric potential. The PAN-C/BTO based flexible sensor is composed of three functional components: carbonized PAN nanofibers as the electrode, BTO NPs embedded in the nanofibers for providing the piezoelectric effect, and the encapsulating PDMS as the friction layer (Figure 4b). PDMS is a kind of commonly used flexible triboelectric material, and it is negative in triboelectric series.[40] When an active object, such as human hand, contacts with the PDMS, triboelectrification occurs at the interface. Simultaneously, the stress caused by contact makes the BTO deform to generate a local piezoelectric potential, enhancing the surface potential of the sensor (Figure 4c). When the object departs away from the surface of the sensor, equivalent positive charge would be induced on the conductive PAN-C/BTO nanofiber layer due to the electrostatic induction effect (Figure 4d). This process accompanies with the charge flowing. Until the active object is far away from the sensor, the electron flowing stops (Figure 4e). As the active object approaches the sensor again, electrons would flow from the ground to the PAN-C/BTO nanofiber layer (Figure 4f). Then the next cycle starts from contacting between the object and the sensor (Figure 4c).

The effect of the BTO nanoparticles on the output performance was investigated as well. In our study, BTO can enhance the output performance of the self-powered pressure sensor (**Figure 5a-b)**. The direction of the piezoelectric polarization of BTO nanoparticles in this system is perpendicular to the axis of PAN-C. To verify this mechanism, the potential

distribution of the PAN-C/BTO nanofiber layer was analyzed by finite-element simulation with the commercial software COMSOL (Figure 5c-d). Simulation studies have shown that when the force is applied, the output performance is enhanced due to the piezoelectric effect on the BTO nanoparticles. As the force increases, the negative charge on the surface and the positive charge in PAN-C increase accordingly (Supplementary Video 1). This mechanism optimizes the output performance by coupling triboelectric charges and piezoelectric charges.

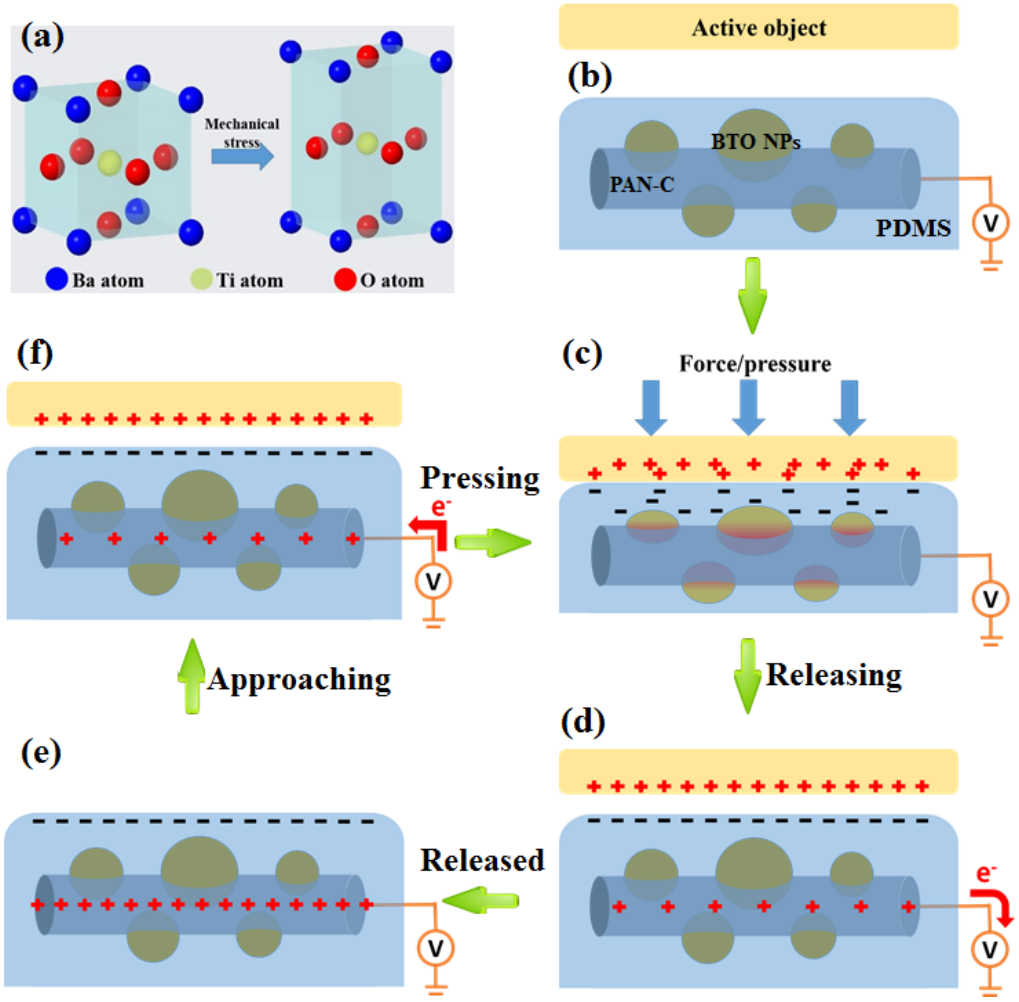

Figure 4. The working mechanism of the PAN-C/BTO based self-powered pressure sensor. a) BTO nanoparticles are poled to create a piezoelectric potential when a mechanical force is applied onto the sensor. b) The original state of the sensor before contacting with an active object. c) The moment of contacting and pressing between the object and the sensor. d) The active object starts to depart from the sensor and the pressure has been released. e) The active

object is far away from the sensor. f) The active object is approaching the sensor and preparing to press on the sensor.

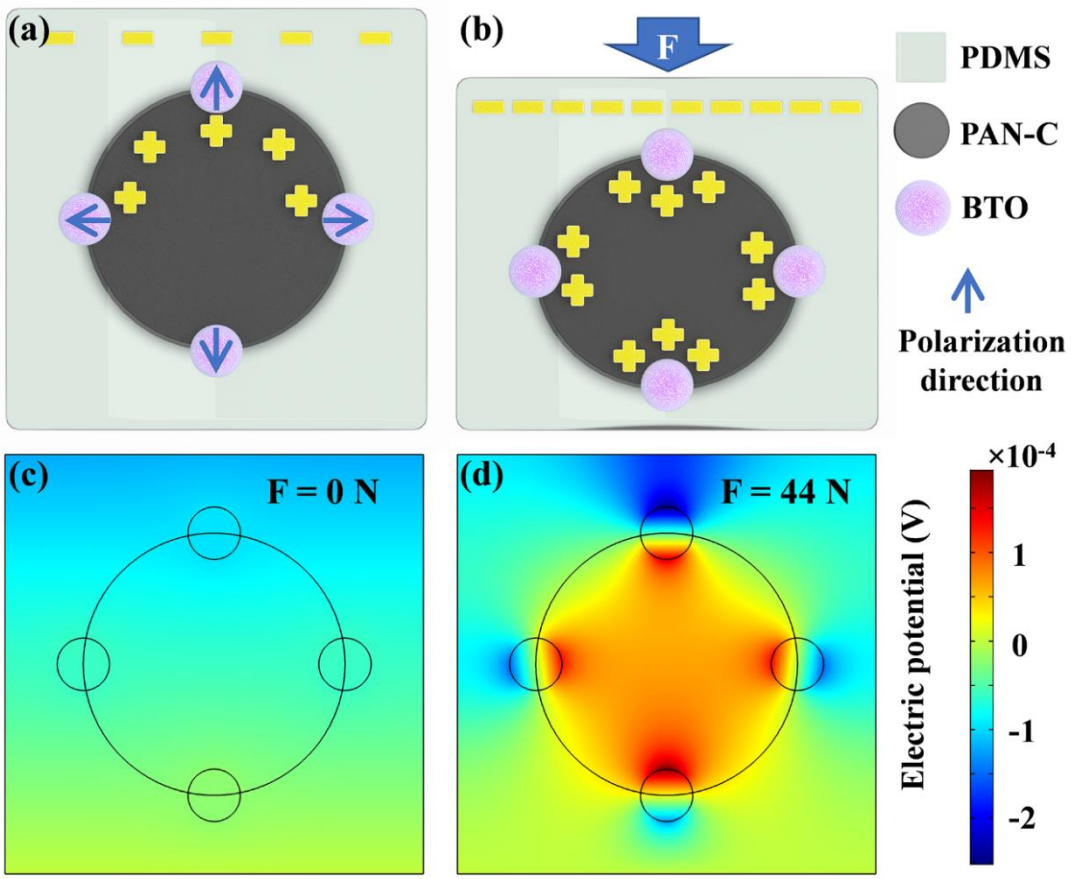

Figure 5. Working mechanism of BTO nanoparticles enhancing the output performance. (a-b) Schematic diagram of the self-powered pressure sensor with F=0 and F = Fx. (c-d) Finite-element simulation of the potential distribution of the PAN-C/BTO nanofiber layer.

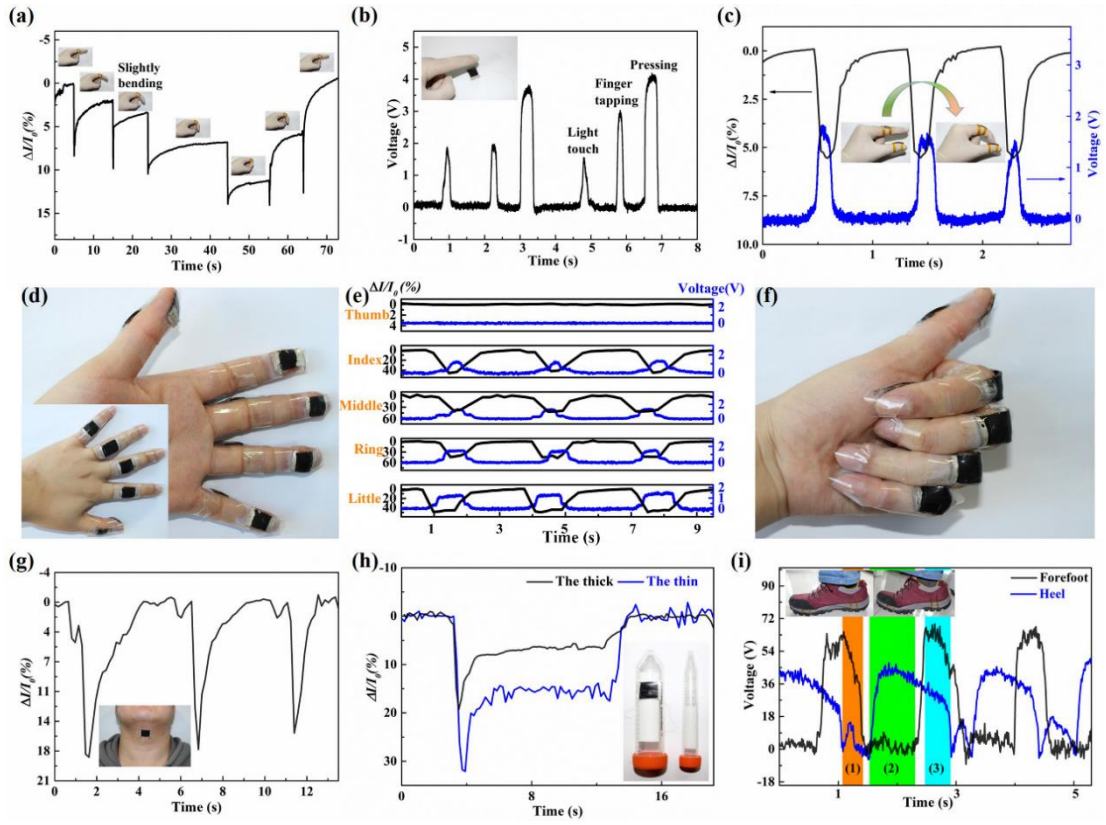

Figure 6. Detection of different human motions and flexural measurement using the flexible dual-function PAN-C/BTO based sensor. a) When the sensor was attached on the knuckle, it can detect different bending degree of the finger knuckle. b) As a self-powered tactile sensor, it can sense different contact strength. c) By combining the two working modes, the sensor on the knuckle (flex sensing mode) and on the fingertip (self-powered pressure sensing mode) could express a pinching motion. (d) A smart sensing system was proposed with integrating two sensors on each finger. It could express different hand gesture, such as (e) finger spray for (f) a "good" gesture. (g) The sensor can detect action of swallowing. (h) The flex sensor can measure the thickness of cylinders during the process of banding onto them due to different curvature radius. (i) When two PAN-C/BTO based self-powered pressure sensors were attached under a shoe, they could detect human walking synergistically. (1) The heel is touching the ground with the forefoot falling. (2) The heel is lifting and the forefoot remains in contact with the ground. (3) The foot has left the floor.

Owing to the outstanding flexibility and versatility, the PAN-C/BTO based sensor has promising applications in wearable devices. Attached on the knuckle of a volunteer, the PAN-C/BTO based flex sensor could be used to capture the subtle motions of human fingers. **Figure 6**a shows a whole bending-extending cycle curve of a finger free movement. In the bending process, a slight bending could be detected sensitively (Supplementary Video 2). In addition to the common bending activities, the finger touch is another important finger activity. With a self-powered force sensing ability, the PAN-C/BTO based sensor could distinguish different strength of touches (Supplementary Video 3). By measuring the open-circuit voltage between the sensor and the ground, the PAN-C/BTO based sensor could sense the strength of finger touch without any external power supply. The PAN-C/BTO based sensor could recognize the light touch, finger tapping and pressing easily (Figure 6b). Based on its multifunction, one sensor was attached on the finger joint to sense the bending motion and another was stuck on the finger pulp to detect the touch movement, simultaneously. A "pinching" gesture could be captured (Figure 6c). The sensor with good modularity could be conveniently integrated into a sensing system. For example, a gesture sensing system comprised of 10 sensors (Figure 6d). Figure 6e shows the curves of fingers' bending-stretching movements, which expressed a "good" gesture language in Figure 6f. $\Delta I/I_0$ curves originated from the signals of the fingers bending (from sensors on the Knuckle back) and voltage curves are signals of finger pulps contacting with palm (from sensors on the finger pads). There is no $\Delta I/I_0$ or voltage signal from the thumb because it was not moved during the course of action. So, two sensors on different positions of one finger could detect the movements of the finger independently, and several modularized sensors could sense more complicated motions synergistically.

As a compact and portable wearable sensor, it also can monitor human health related motion such as swallowing (Figure 6g). When swallowing, the larynx is raised and pressed forward and the laryngeal passage is blocked to prevent the food entering the trachea.[41] During this

process, laryngeal prominence moves up and down. The PAN-C/BTO based senor was stuck on the laryngeal prominence of a male volunteer. When swallowing, the sensor was bent with the laryngeal prominence lifting. The sensor totally detected 3 swallowing actions during 13 seconds. So, the sensor had the potential in health monitoring to detect the eating process of patient. The PAN-C/BTO based sensor also could distinguish the material shape and geometry based on the bending action. By sticking the flex sensors onto the surface of two cylinders with different diameters, respectively, the flex sensor had different bending deformation to induce differentiated current signals (Figure 6h).

Figure 6i presents the real-time voltage change of two PAN-C/BTO based sensors attached at the bottom of a shoe. One sensor was attached under the forefoot and another under the heel so that they could sense the human's gait. They could work as self-powered tactile sensors to detect the contact between the sole and the smooth marble floor. The marble floor with a smooth and clean surface could fully contact with the PDMS sensor. It was triboelectro-positive relative to PDMS. Generally, during human walking, the heel will touch the ground first with the forefoot falling and this process (1) is short in time. In process (2), the heel lifts and the forefoot remains in contact with the ground. So the sensor under the heel has a higher voltage signal and the one under the forefoot keeps a low triboelectric potential. This process takes longer time because the other leg is moving forward during the forefoot keeps on the ground. In process (3), the foot leaves the floor and both sensors have high triboelectric outputs. In this way, the PAN-C/BTO based sensors detected a complete process of one step from foot falling down to lifting the ground. If more sensors are integrated under soles to form a sensing system, they can detect the gait of different people because of the different plantar force distribution. So, the sensor is expected to use as multifunctional sensor for human health monitoring.

4. CONCLUSIONS

In summary, we have fabricated a wearable and flexible sensor via a facile electrospinning, carbonization and encapsulation process. Based on the integration of piezoresistive, triboelectric and piezoelectric effect, it had the advantages of multifunction, modularization, and high sensitivity. For flexural sensing, the PAN-C/BTO based sensor had a gauge factor of 1.12 deg^{-1} from 58.9° to 120.2° and a working range of 28°~150°. For self-powered force sensing, it had a high sensitivity of 1.44 $V \cdot N^{-1}$ in the range of 0.15~25 N. Furthermore, the PAN-C/BTO based sensor had a high stability (> 60,000 cycles) when working as either flex sensor or force sensor. According the finite-element model, the high signal strength of self-powered force senor was originated from the triboelectric output and piezoelectric output of the BTO NPs. The sensors could be used for bending and tactile sensing, and be assembled into a gesture sensing system based on their modularity. As a medical monitoring sensor, it could be used to monitor swallowing motion of human or perform basic bending measurement. These sensors also could be integrated into soles to capture the human gait. Based on the numerous advantages, the PAN-C/BTO based sensor has broad application prospects in future wearable electronics.

ASSOCIATED CONTENT

Supporting Information.

The supporting Information is available free of charge on the ACS Publications website at DOI: SEM image of as-spun PAN/BTO nanofibers; photos of elelctrospun nanofiber film before and after carbonization; TEM image of BTO NPs; water-proof of the PAN-C/BTO based flex sensor; real-time $\Delta I/I_0$ curves of PAN-C based flex sensor; real-time $\Delta I/I_0$ curves of PAN-C based flex sensor subjected to a horizontal impulse force; real-time V_{oc} curves of the sensor with/without bending under pressure; video for dynamic change process of potential on the sensor surface during applying pressure; video for sensing of finger bending; video for self-powered force

sensing.

AUTHOR INFORMATION

Corresponding Author

*E-mail: lilinlin@binn.cas.cn. Tel: +86-10-82854770. Fax:+86-140-82854800

*E-mail: zhangyan@uestc.edu.cn. Tel: +86-28-83200098

ORCID

Linlin Li: 0000-0003-1041-4533

Notes

The authors declare no competing financial interest.

ACKNOWLEDGMENTS

The work was supported by the National Natural Science Foundation of China (No. 81471784), Nature Science Foundation of Beijing (2172058), the Youth Innovation Promotion Association of the Chinese Academy of Sciences (2015023), and the "Thousands Talents" program for pioneer researcher and his innovation team, China.

REFERENCES

(1) Chortos, A.; Liu, J.; Bao, Z. Pursuing Prosthetic Electronic Skin. *Nat. Mater.* **2016**, *15*, 937−950.

(2) Chou, H.-H.; Nguyen, A.; Chortos, A.; To, J. W. F.; Lu, C.; Mei, J.; Kurosawa, T.; Bae, W.-G.; Tok, J. B. H.; Bao, Z. A Chameleon-Inspired Stretchable Electronic Skin with Interactive Colour Changing Controlled by Tactile Sensing. *Nat. Comm.* **2015**, *6*, No. 8011.

(3) Lee, S.; Reuveny, A.; Reeder, J.; Lee, S.; Jin, H.; Liu, Q.; Yokota, T.; Sekitani, T.; Isoyama, T.; Abe, Y.; Suo, Z.; Someya, T. A Transparent Bending-Insensitive Pressure Sensor. *Nat. Nanotechnol.* **2016**, *11*, 472−478.

(4) Lipomi, D. J.; Vosgueritchian, M.; Tee, B. C. K.; Hellstrom, S. L.; Lee, J. A.; Fox, C. H.; Bao, Z. Skin-like Pressure and Strain Sensors Based on Transparent Elastic Films of Carbon Nanotubes. *Nat. Nanotechnol.* **2011**, *6*, 788−792.

(5) Wang, J.; Li, S.; Yi, F.; Zi, Y.; Lin, J.; Wang, X.; Xu, Y.; Wang, Z. L. Sustainably Powering Wearable Electronics Solely by Biomechanical Energy. *Nat. Comm.* **2016**, *7*, No. 12744.

(6) Chen, J.; Huang, Y.; Zhang, N.; Zou, H.; Liu, R.; Tao, C.; Fan, X.; Wang, Z. L. Micro-cable Structured Textile for Simultaneously Harvesting Solar and Mechanical Energy. *Nat. Energy* **2016**, *1*, No. 16138.

(7) Gao, Y. P.; Gu, J. L.; Li, L.; Zhao, W. R.; Li, Y. S. Synthesis of Gold Nanoshells Through Improved Seed-mediated Growth Approach: Brust-like, In Situ Seed Formation. *Langmuir* **2016**, *32*, 2251−2258.

(8) Ren, X.; Pei, K.; Peng, B.; Zhang, Z.; Wang, Z.; Wang, X.; Chan, P. K. L. A Low-Operating-Power and Flexible Active-Matrix Organic-Transistor Temperature-Sensor Array. *Adv. Mater.* **2016**, *28*, 4832−4838.

(9) Ma, Y.; Liu, N.; Li, L.; Hu, X.; Zou, Z.; Wang, J.; Luo, S.; Gao, Y. A Highly Flexible and Sensitive Piezoresistive Sensor Based on MXene with Greatly Changed Interlayer Distances. *Nat. Comm.* **2017**, *8*, No. 1207.

(10) Wang, C.; Li, X.; Gao, E.; Jian, M.; Xia, K.; Wang, Q.; Xu, Z.; Ren, T.; Zhang, Y. Carbonized Silk Fabric for Ultrastretchable, Highly Sensitive, and Wearable Strain Sensors. *Adv. Mater.* **2016**, *28*, 6640−6648.

(11) Khim, D.; Ryu, G.-S.; Park, W.-T.; Kim, H.; Lee, M.; Noh, Y.-Y. Precisely Controlled Ultrathin Conjugated Polymer Films for Large Area Transparent Transistors and Highly

Sensitive Chemical Sensors. *Adv. Mater.* **2016**, *28*, 2752−2759.

(12) Li, Z.; Wang, Z. L., Air/Liquid-pressure and Heartbeat-Driven Flexible Fiber Nanogenerators as A Micro/Nano-Power Source or Diagnostic Sensor. *Adv. Mater.* **2011**, *23*, 84−89.

(13) Pu, X.; Guo, H.; Chen, J.; Wang, X.; Xi, Y.; Hu, C.; Wang, Z. L. Eye Motion Triggered Self-Powered Mechnosensational Communication System Using Triboelectric Nanogenerator. *Sci. Adv.* **2017**, *3*, e1700694

(14) Yao, S.; Zhu, Y. Wearable Multifunctional Sensors Using Printed Stretchable Conductors Made of Silver Nanowires. *Nanoscale* **2014**, *6*, 2345−2352.

(15) Gong, S.; Schwalb, W.; Wang, Y.; Chen, Y.; Tang, Y.; Si, J.; Shirinzadeh, B.; Cheng, W. A Wearable and Highly Sensitive Pressure Sensor with Ultrathin Gold Nanowires. *Nat. Comm.* **2014**, *5*, No. 3132.

(16) Shin, S.-H.; Ji, S.; Choi, S.; Pyo, K.-H.; Wan An, B.; Park, J.; Kim, J.; Kim, J.-Y.; Lee, K.-S.; Kwon, S.-Y.; Heo, J.; Park, B.-G.; Park, J.-U. Integrated Arrays of Air-Dielectric Graphene Transistors as Transparent Active-Matrix Pressure Sensors for Wide Pressure Ranges. *Nat. Comm.* **2017**, *8*, No. 14950.

(17) Wang, Z.; Jiang, R.; Li, G.; Chen, Y.; Tang, Z.; Wang, Y.; Liu, Z.; Jiang, H.; Zhi, C. Flexible Dual-mode Tactile Sensor Derived from Three-dimensional Porous Carbon Architecture. *ACS Appl. Mater. Inter.* **2017**, *9*, 22685−22693.

(18) Gao, Y.; Ota, H.; Schaler, E. W.; Chen, K.; Zhao, A.; Gao, W.; Fahad, H. M.; Leng, Y.; Zheng, A.; Xiong, F.; Zhang, C.; Tai, L.-C.; Zhao, P.; Fearing, R. S.; Javey, A. Wearable Microfluidic Diaphragm Pressure Sensor for Health and Tactile Touch Monitoring. *Adv. Mater.* **2017**, *29*, 1701985.

(19) Park, D. Y.; Joe, D. J.; Kim, D. H.; Park, H.; Han, J. H.; Jeong, C. K.; Park, H.; Park, J. G.; Joung, B.; Lee, K. J. Self-Powered Real-Time Arterial Pulse Monitoring Using Ultrathin

Epidermal Piezoelectric Sensors. *Adv. Mater.* **2017**, *29*, 1702308.

(20) Chen, Z.; Wang, Z.; Li, X.; Lin, Y.; Luo, N.; Long, M.; Zhao, N.; Xu, J.-B. Flexible Piezoelectric-Induced Pressure Sensors for Static Measurements Based on Nanowires /Graphene Heterostructures. *ACS Nano* **2017**, *11*, 4507−4513.

(21) Lin, Z.; Chen, J.; Li, X.; Zhou, Z.; Meng, K.; Wei, W.; Yang, J.; Wang, Z. L. Triboelectric Nanogenerator Enabled Body Sensor Network for Self-Powered Human Heart-Rate Monitoring. *ACS Nano* **2017**, *11*, 8830−8837.

(22) Seung, W.; Gupta, M. K.; Lee, K. Y.; Shin, K.-S.; Lee, J.-H.; Kim, T. Y.; Kim, S.; Lin, J.; Kim, J. H.; Kim, S.-W. Nanopatterned Textile-Based Wearable Triboelectric Nanogenerator. *ACS Nano* **2015**, *9*, 3501−3509.

(23) Guo, W.; Zhang, X.; Yu, X.; Shu, W.; Qiu, J.; Tang, W.; Li, L.; Liu, H.; Wang, Z. L. Self-Powered Electrical Stimulation for Enhancing Neural Differentiation of Mesenchymal Stem Cells on Graphene-Poly(3,4-ethylenedioxythiophene) Hybrid Microfibers. *ACS Nano*, **2016**, *10*, 5086–5095.

(24) Luo, J.; Fan, F. R.; Zhou, T.; Tang, W.; Xue, F.; Wang, Z. L. Ultrasensitive Self-Powered Pressure Sensing System. *Extreme Mechanics Letters* **2015**, *2*, 28−36.

(25) Wang, H.; Wu, H.; Hasan, D.; He, T.; Shi, Q.; Lee, C. Self-Powered Dual-Mode Amenity Sensor Based on the Water–Air Triboelectric Nanogenerator. *ACS Nano* **2017**, *11*, 10337−10346.

(26) Zhang, C.-L.; Yu, S.-H. Nanoparticles Meet Electrospinning: Recent Advances and Future Prospects. *Chem. Soc. Rev.* **2014**, *43*, 4423−4448.

(27) Lin, Z.-H.; Yang, Y.; Wu, J. M.; Liu, Y.; Zhang, F.; Wang, Z. L. $BaTiO_3$ Nanotubes-Based Flexible and Transparent Nanogenerators. *J. Phys. Chem. Lett.* **2012**, *3*, 3599−3604.

(28) Shin, S.-H.; Kim, Y.-H.; Lee, M. H.; Jung, J.-Y.; Nah, J. Hemispherically Aggregated

$BaTiO_3$ Nanoparticle Composite Thin Film for High-Performance Flexible Piezoelectric Nanogenerator. *ACS Nano* **2014**, *8*, 2766−2773.

(29) Alluri, N. R.; Chandrasekhar, A.; Vivekananthan, V.; Purusothaman, Y.; Selvarajan, S.; Jeong, J. H.; Kim, S.-J. Scavenging Biomechanical Energy Using High-Performance, Flexible $BaTiO_3$ Nanocube/PDMS Composite Films. *ACS Sustain.Chem. Eng.* **2017**, *5*, 4730−4738.

(30) Zhuang, Y.; Li, F.; Yang, G.; Xu, Z.; Li, J.; Fu, B.; Yang, Y.; Zhang, S. Fabrication and Piezoelectric Property of $BaTiO_3$ Nanofibers. *J. Am. Ceram. Soc.* **2014**, *97*, 2725−2730.

(31) Bowland, C. C.; Malakooti, M. H.; Sodano, H. A. Barium Titanate Film Interfaces for Hybrid Composite Energy Harvesters. *ACS Appl. Mater. Inter.* **2017**, *9*, 4057−4065.

(32) Ávila, H. A.; Ramajo, L. A.; Góes, M. S.; Reboredo, M. M.; Castro, M. S.; Parra, R. Dielectric Behavior of Epoxy/$BaTiO_3$ Composites Using Nanostructured Ceramic Fibers Obtained by Electrospinning. *ACS Appl. Mater. Inter.* **2013**, *5*, 505−510.

(33) Yan, J.; Jeong, Y. G. High Performance Flexible Piezoelectric Nanogenerators Based On $BaTiO_3$ Nanofibers in Different Alignment Modes. *ACS Appl. Mater. Inter.* **2016**, *8*, 15700-15709.

(34) Mahadeva, S. K.; Walus, K.; Stoeber, B. Piezoelectric Paper Fabricated via Nanostructured Barium Titanate Functionalization of Wood Cellulose Fibers. *ACS Appl. Mater. Inter.* **2014**, *6*, 7547-7553.

(35) Ferrari, A. C.; Robertson, J. Resonant Raman Spectroscopy of Disordered, Amorphous, and Diamondlike Carbon. *Phys. Rev. B* **2001**, *64*, 075414.

(36) Yu, W.; Santiago-Aviles, J. J.; Furlan, R.; Ramos, I. Pyrolysis Temperature and Time Dependence of Electrical Conductivity Evolution for Electrostatically Generated Carbon Nanofibers. *IEEE T. Nanotechnol.* **2003**, *2*, 39−43.

(37) Wang, Y.; Serrano, S.; Santiago-Avilés, J. J. Raman Characterization of Carbon Nanofibers

Prepared Using Electrospinning. *Synthetic Met.* **2003**, *138*, 423−427.

(38) Jung, S.; Lee, J.; Hyeon, T.; Lee, M.; Kim, D.-H. Fabric-Based Integrated Energy Devices for Wearable Activity Monitors. *Adv. Mater.* **2014**, *26*, 6329−6334.

(39) Pu, J.; Wang, X.; Xu, R.; Komvopoulos, K. Highly Stretchable Microsupercapacitor Arrays with Honeycomb Structures for Integrated Wearable Electronic Systems. *ACS Nano* **2016**, *10*, 9306−9315.

(40) Diaz, A. F.; Felix-Navarro, R. M. A Semi-Quantitative Tribo-electric Series for Polymeric Materials: the Influence of Chemical Structure and Properties. *J.Electrost.* **2004**, *62*, 277−290.

(41) Iva, J.; James, L. C.; Ervin, S. Decoding Human Swallowing via Electroencephalography: A State-of-the-Art Review. *J. Neural Eng.* **2015**, *12*, 051001 (15pp).

Table of Contents (TOC)